Investigation of laser-driven proton acceleration using ultra-short, ultra-intense laser pulses

S. Fourmaux, S. Buffechoux, B. Albertazzi, D. Capelli, A. Lévy et al.

Citation: Phys. Plasmas **20**, 013110 (2013); doi: 10.1063/1.4789748
View online: http://dx.doi.org/10.1063/1.4789748
View Table of Contents: http://pop.aip.org/resource/1/PHPAEN/v20/i1
Published by the American Institute of Physics.

Investigation of laser-driven proton acceleration using ultra-short, ultra-intense laser pulses

S. Fourmaux,[1,a)] S. Buffechoux,[1,2] B. Albertazzi,[1,2] D. Capelli,[2,3] A. Lévy,[2] S. Gnedyuk,[1] L. Lecherbourg,[4] P. Lassonde,[1] S. Payeur,[1] P. Antici,[2,3] H. Pépin,[1] R. S. Marjoribanks,[4] J. Fuchs,[2] and J. C. Kieffer[1]

[1]*INRS-EMT, Université du Québec, 1650 Lionel Boulet, Varennes, Québec J3X 1S2, Canada*
[2]*LULI, UMR 7605, CNRS – CEA – Université Paris 6 – École Polytechnique, 91128 Palaiseau, France*
[3]*Dipartimento SBAI, Sapienza, Universita di Roma, Via Scarpa 16, 00161 Roma, Italy*
[4]*Department of Physics and Institute for Optical Sciences, University of Toronto, Toronto, Ontario M5S 1A7, Canada*

(Received 23 December 2012; accepted 14 January 2013; published online 29 January 2013)

We report optimization of laser-driven proton acceleration, for a range of experimental parameters available from a single ultrafast Ti:sapphire laser system. We have characterized laser-generated protons produced at the rear and front target surfaces of thin solid targets (15 nm to 90 μm thicknesses) irradiated with an ultra-intense laser pulse (up to 10^{20} W · cm^{-2}, pulse duration 30 to 500 fs, and pulse energy 0.1 to 1.8 J). We find an almost symmetric behaviour for protons accelerated from rear and front sides, and a linear scaling of proton energy cut-off with increasing pulse energy. At constant laser intensity, we observe that the proton cut-off energy increases with increasing laser pulse duration, then roughly constant for pulses longer than 300 fs. Finally, we demonstrate that there is an optimum target thickness and pulse duration. © *2013 American Institute of Physics*. [http://dx.doi.org/10.1063/1.4789748]

I. INTRODUCTION

High-power laser technology improvements since the 1980 s today permit focused intensities up to the range of 10^{21} W · cm^{-2}. Thus, existing laser facilities allow the scientific community to explore fundamental physics and applications promising for society, using laser-matter interactions in the ultra-relativistic regime. Among these applications, sources of electromagnetic radiation[1,2] and energetic particles[3,4] are now sufficiently mature that they could complement current conventional sources such as synchrotrons or accelerators.

Acceleration of energetic ions by laser-plasma interactions, through the production of hot electrons and the generation of very strong ambipolar fields, dates back to nanosecond CO_2 laser-plasma studies in the 1970s. Hot electron sheath production depends on large values of $I_{laser} \times \lambda^2$ (where I_{laser} is the laser peak intensity on target, and λ is the laser wavelength), and on steep plasma gradients, both of which were produced in nanosecond interactions at 10 μm wavelength, ponderomotively steepened.[5,6] The impact of hot electrons in driving the expansion of ions was quantified as well, with the use of pairs of foils.[7]

In the last ten years, energetic ion beams have been produced from thin metallic foils irradiated by ultra-intense ultra-short laser pulses.[8–10] Laser-driven ion beams take advantage of acceleration in the huge electric fields that can be obtained in a plasma. Fields exceeding several TV/m can be obtained, which is well beyond the breakdown-voltage, which limits conventional accelerators (~100 MV/m). The source is very compact, as with such fields, ions can be accelerated to MeV energies over a mere few micrometers. These ion beams also exhibit outstanding characteristics: low emittance,[11] low divergence,[12] and short bunch-duration. These properties are of interest in fundamental plasma research such as proton-radiography,[13] warm dense matter generation,[14] or ion-driven fast ignition.[15] They also bode well for applications-experiments in areas such as isotope production,[16] or hadron therapy.[17] However, further progress is needed on the beam divergence, output current, and maximum energy (i.e., cut-off energy), to improve the prospects for applications.

At the laser intensities currently available, and for most typical laser-matter interaction conditions, ions are primarily accelerated by the so-called target normal sheath acceleration (TNSA) process. In this mechanism, relativistic electrons are produced by the laser pulse at the laser-irradiated (front) surface. Penetrating freely through the target, these energetic electrons establish space-charge sheath fields at both surfaces, which then pull ions outward in both directions,[18] as illustrated in Figure 1. As long as plasma gradients on target surfaces remain sufficiently steep (i.e., scale lengths remain small),[19] the ambipolar sheath is nearly planar, the electric-field vectors are well defined, and the beam of accelerated ions has its smallest emittance. Where the plasma has significantly evolved from the surface, the aspect ratio of the sheath changes, and the increased divergence means both a reduced maximum ion energy and an increased beam emittance. Where the number of energetic electrons is a small fraction of the total, Debye shielding in the dense plasma of the foil means that ions are extracted only from a thin region near the surface. When no specific cleaning of the surface has been performed, it is protons which are predominantly accelerated, because of their low charge-to-mass

a)Electronic mail: fourmaux@emt.inrs.ca.

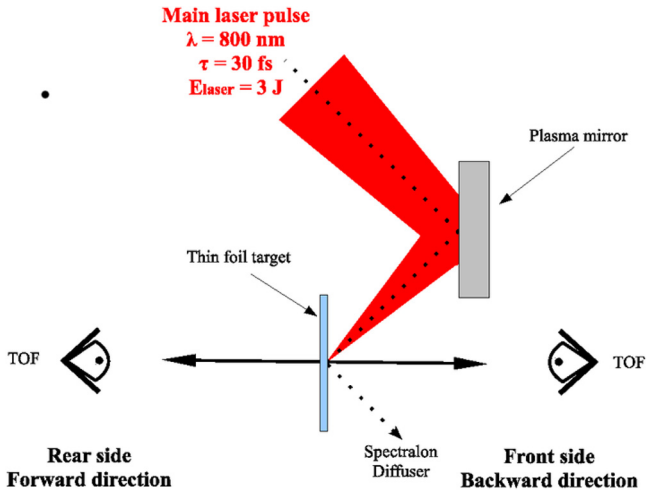

FIG. 1. Experimental set-up depicted in the laser plane-of-incidence. The main laser pulse is incident at 45°, on both the plasma mirror and the target, P-polarized for both. Charged-particle TOF diagnostics are positioned on the target surface normal-axis, measuring both front- and rear-side accelerated-proton beams. The target reflectivity is measured with the help of a Spectralon diffuser located in the specular beam path.

ratio.[20] These originate from hydrocarbon contaminants that are naturally adsorbed on target surfaces, in a matter of seconds, even under moderate vacuum. Using TNSA, the maximum proton cut-off energy that has been achieved to date with a high power laser system is 67 MeV,[21] and the associated conversion efficiency is on the order of 1-2%.[22]

Alternatively to TNSA, other acceleration mechanisms have been identified and studied: radiation pressure acceleration (RPA)[23–27] and break-out afterburner (BOA).[28–30] In contrast to TNSA, by these mechanisms, the laser energy is efficiently transferred to the ions within the target volume itself. In the RPA process, the light-pressure of a linearly polarized laser pulse exceeding $10^{23}\,\mathrm{W\cdot cm^{-2}}$, less for circularly polarized light, delivered onto an ultra-thin foil, accelerates the foil under the focal spot as a plasma slab. In the BOA process, beyond a laser intensity of $5\times10^{19}\,\mathrm{W\cdot cm^{-2}}$, the laser directly penetrates a normally over-dense target, because it appears under-dense in the relativistic regime. Strong volumetric heating of virtually all plasma electrons enables the accelerated ions to reach high energies. These mechanisms require very demanding laser pulse characteristics, in context of present-day technologies: for example, ultra-high laser intensities, and ultra-high intensity contrast-ratio between the laser pulse itself and any irradiance delivered in advance of the pulse.

In this paper, we concentrate on TNSA as the main acceleration mechanism for the current laser conditions. We analyze several strategies that have the potential to increase the maximum ion beam energy in the ultra-high intensity regime. We concentrate on ion acceleration using high-repetition-rate femtosecond Ti:Sapphire laser since these are the common commercial table-top laser system and are promising for widespread applications. Indeed, small footprint size, moderate cost, and high repetition rate are important parameters to push forward the relevance and the competitiveness of laser driven proton beams.

In Sec. II, the laser configuration and the experimental set up are described. Section III reports on ion beams produced from the rear and the front sides of thin targets. We analyze the proton energy cut-off behaviour as the laser pulse-energy is modified while keeping the laser pulse-duration constant. The evolution of maximum proton-energy as a function of laser-pulse duration is also determined, keeping laser intensity constant. We demonstrate that, as predicted for lower intensity and longer pulse duration,[22] proton-beam cut-off energy depends linearly on pulse energy as pulse duration is kept constant, and logarithmically on pulse duration as laser intensity is kept constant. Section III concludes with a discussion of the trade offs to be made between laser intensity and pulse duration, in order to optimize absorption, control hot-electron number, electron temperature, and evolved-plasma scale-length, all ultimately to maximize proton energy temperature.

II. EXPERIMENTAL SET-UP

A. Laser system

Experiments were performed using the 100-TW-class laser system at the Advanced Laser Light Source (ALLS) facility located at INRS-EMT.[31] This Ti:Sapphire-based laser system has a central wavelength of 800 nm and a 55 nm bandwidth that allows compression of the pulse down to 25 fs duration full width at half maximum (FWHM). A deformable mirror coupled to a Shack-Hartmann wavefront sensor is mounted in vacuum after the pulse compressor to correct aberrations that originate in the laser chain. Using an *f*/3 off-axis parabola, the beam is focused to $5.6\pm0.4\,\mu$m diameter (FWHM), with 30% of laser energy delivered within this diameter.

To increase the laser pulse temporal contrast between the peak intensity and the nanosecond-timescale pedestal or prepulse, a saturable absorber is used before injection of the laser pulse into the regenerative amplifier (this is achieved just before the stretcher). It supports a contrast ratio close to 10^{10} for times up to 20 ps before the peak intensity.[32] Since a laser-pulse nanosecond pedestal or pre-pulse both inhibit proton acceleration from thin targets, their energy should be kept as low as possible. To further suppress pre-irradiation, an anti-reflection-coated planar plasma-mirror is placed in the path of the converging *f*/3 beam, 7 mm before final focus. This produced a laser fluence of $\sim50\,\mathrm{J\cdot cm^{-2}}$ on the plasma mirror surface. The measured net reflectivity using the plasma mirror is 60% for the laser pulse at nominal energy, but less than 0.5% for low-intensity light, before optical breakdown. From this, we infer an improvement in the laser-pulse intensity-contrast ratio of around 10^2. Based on the measured form of the intrinsic pulse of our system, and assuming a breakdown-intensity of $2\times10^{14}\,\mathrm{W\cdot cm^{-2}}$, our plasma mirror should be able to inhibit by 2 orders of magnitude the rising edge of our laser pulse, for times prior to $\sim$1 ps before the peak of the laser pulse.[33]

Given our plasma mirror reflectivity, the maximum laser energy on target is nominally $E_{laser}=1.8\,\mathrm{J}$. With a standard laser pulse-duration $\tau_{laser}\sim30\,\mathrm{fs}$, peak intensity on target is close to $I_{laser}=10^{20}\,\mathrm{W\cdot cm^{-2}}$ during these

experimental series. For a convenience of the set-up, and in order to maximize laser-plasma absorption, the laser angle-of-incidence on target is fixed at 45° and P-polarization is used (see Fig. 1).

B. Diagnostics

In the target schematic of Fig. 1, we define the target front side as being the irradiated side and label the non-irradiated side as the target rear side. The forward direction we take to be along the direction of propagation of the laser main beam, and the backward direction the opposite direction.

In order to measure the energy of protons beams directed from both front and rear surfaces of the target after laser irradiation, two time-of-flight (TOF) spectrometers are placed along the target normal axis, fore and aft of the target. These served to characterize ion energy distributions, on a single-shot basis, in both the forward and the backward directions. The TOF spectrometer consists of a long evacuated tube leading to a plastic fast scintillator (EJ-212, 1 mm thick, 0.9 ns typical rise time) exposed to a 90° off-angle photomultiplier tube (PMT).[34] The scintillator is protected by a light-tight Al filter (2 μm thick). The distance from target to scintillators is 1.8 and 2.1 m, directed at the target front and rear sides, respectively. We use a fast digital oscilloscope (bandwidth 500 MHz) to record the PMT signal, producing a resolution better than 7% in proton energy measurements, for energies up to 15 MeV. In order to measure the highest energy protons, which are emitted into a narrow cone along the target normal axis,[35] the TOF diagnostic axis is carefully aligned to the target normal axis.

To characterize the plasma generation, several diagnostics are used. The expansion of the critical-density, following irradiation, is characterized from shadowgraphy. For this, a low energy (~100 μJ) 40 fs, 800 nm, probe pulse with timing adjustable relative to the main laser pulse is used. This probe pulse propagated in the main laser pulse plane of incidence, at 90° angle-of-incidence (i.e., grazing along the target surface), and light transmitted through the plasma profile is imaged using a lens and CCD camera, and an interference filter centered at 800 nm. The reflection efficiency for the main laser pulse from the target is measured from diffuse reflection of laser light striking a Spectralon™ diffuser set to intercept the specularly reflected beam, and recorded by a calibrated CCD.

For targets, we used 15 and 30-nm-thick etched silicon nitride (SiN) membranes, to ensure the best flatness. An aluminum coating of variable thickness is sometimes deposited on top of the 30 nm thick membrane, yielding total thicknesses ranging from 30 nm to 1 μm. The targets are aligned at best focus with precision better than 10 μm, less than a Rayleigh range for the focussed beam (~90 μm). Hereafter, target thickness refers to total thickness, membrane and any coating, together. For targets thicker than 1 μm, commercially available aluminum foils are used.

III. RESULTS AND DISCUSSION

A. Experimental characterization of laser-plasma interaction

Shadowgrams of plasma formation (Figure 2) show that plasma expansion is generated from both front and rear sides essentially simultaneously, for thinner targets (less than 2 μm) and its expansion velocity (0.1 μm/ps) corresponds roughly to the ion acoustic velocity in a quasineutral plasma, which for a mean temperature of 100 eV is ~0.03 μm/ps.

Using the Spectralon diffuser, we were able to measure the reflection efficiency of the main laser pulse as function of the pulse duration (with fixed energy pulse). In Figure 3(a), we see that the reflectivity of the target is maximized for a pulse of about 100 fs. Longer than this duration, a long-scale-length plasma has evolved, and more-efficiently absorbs the laser. Shorter than 100 fs, the reflectivity decreases. This may be due to high ponderomotive force, non specular reflection, or energy conversion in harmonics.

Finally, we have looked at the sensitivity of the maximum proton energy to laser-alignment problems and focusing of the laser beam. We measure the proton cut-off energy as a function of the best focusing distance from the target position (with fixed energy and pulse duration). The corresponding intensity range assuming a smooth focal spot is indicated on the upper horizontal axis. We see in Figure 3(b) that a defocusing of 100 μm of the laser-spot results in a reduction of 25% of the maximum proton cut-off energy, while for defocusing of 300 μm, the cut-off energy is reduced by 30%. The Rayleigh range is 90 μm. As mentioned before,

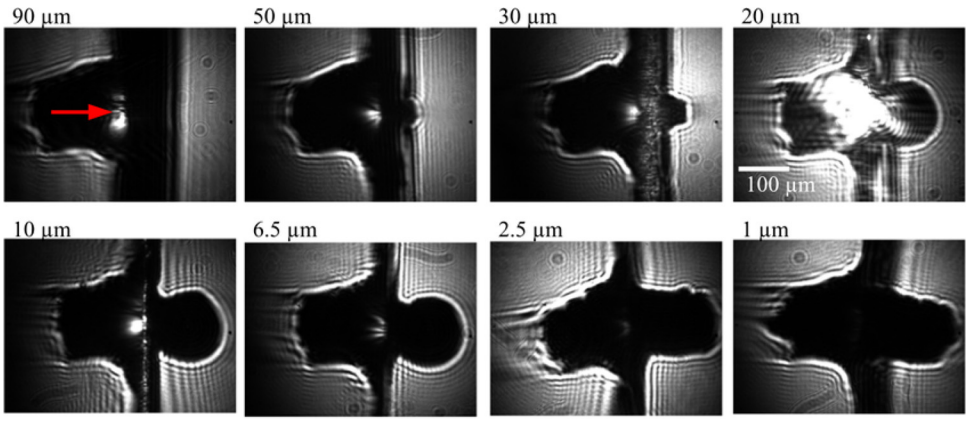

FIG. 2. Shadowgraphy of a series of targets of different thicknesses ranging from 90 μm down to 1 μm. Shadowgraphy probe pulse arrives 1 ns after laser irradiation by a 100 fs laser pulse of intensity 5.7 10^{19} W · cm^{-2}. The red arrow shows the main laser pulse incident direction (front side is on the left for every shadowgraph image). The magnification is identical for all images.

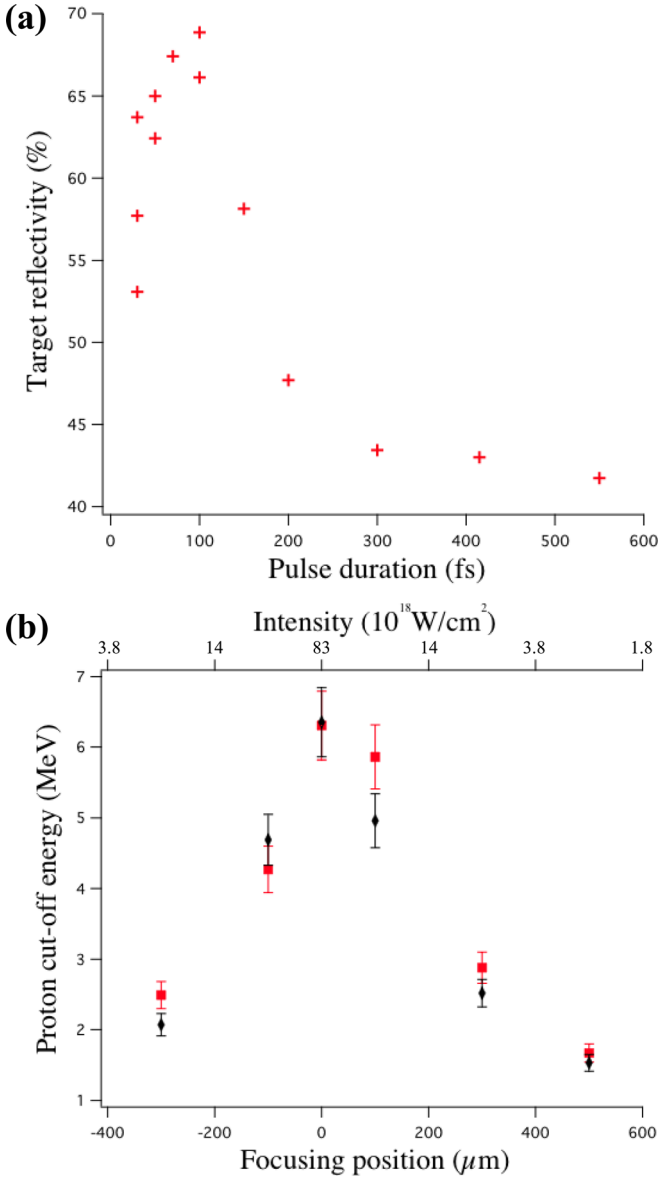

FIG. 3. (a) Reflectivity of a 120 nm Al target irradiated with a 1.8 J laser pulse vs pulse duration. (b) Proton cut-off energy for a 120 nm Al target and 30 fs laser pulse vs defocusing laser position. Results are obtained when using a plasma mirror. Front side protons are indicated with red squares, rear side accelerated protons with black diamonds.

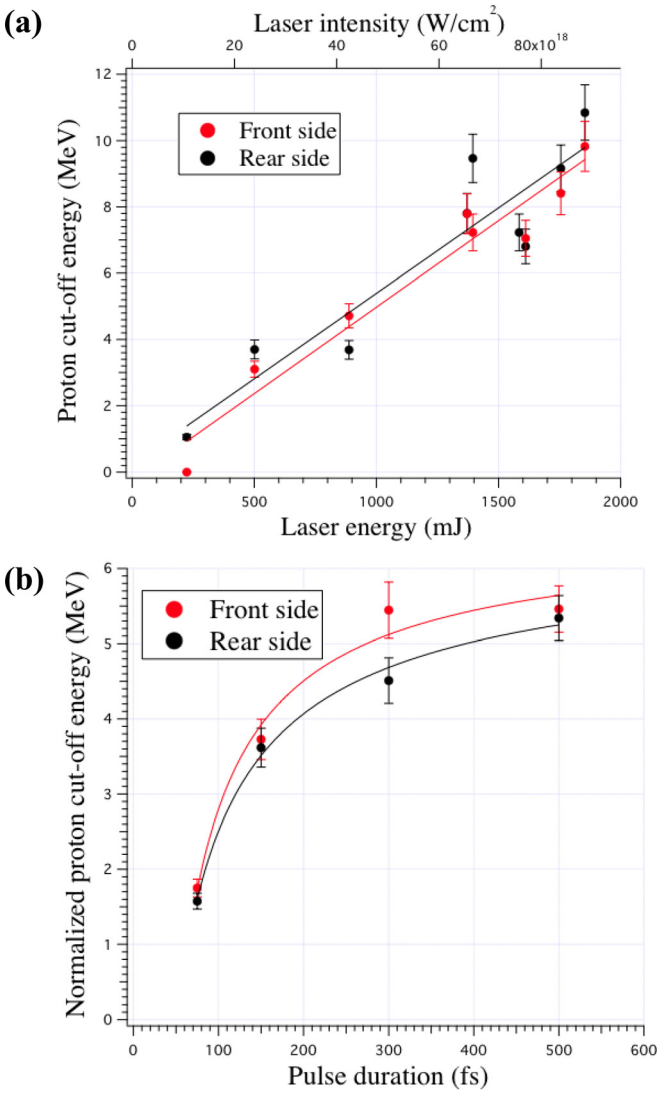

FIG. 4. (a) Cut-off energy for accelerated protons from the target front and rear side versus on-target laser energy using a 30 fs pulse duration. The continuous lines correspond to the linear fit (red line for front side and black line for rear side). (b) Cut-off energy for accelerated protons from the target front and rear side versus laser pulse duration. Laser intensity is kept constant and equal to 6.1×10^{18} W · cm^{-2}. The continuous lines correspond to power-law fit (red line for front side and black line for rear side). In both figures, the target thickness is 120 nm.

the alignment precision is 10 μm; thus, the alignment precision influence on the determination of the proton cut-off energy can be neglected.

B. Dependence of proton-energy cut-off on laser energy, pulse duration, and target thickness

Figure 4 shows the variation of proton beam cut-off energy for both, front-side and rear-side protons, when modifying either the laser energy (with fixed laser pulse duration, see Fig. 4(a)) or pulse duration (with fixed laser intensity, see Fig. 4(b)). In both cases, the target thickness is 120 nm. Figure 4 shows that protons accelerated in the forward and the backward directions have a very similar cut-off energy, as already demonstrated by Ceccotti *et al.*:[36] under high temporal-contrast conditions, there is no pre-pulse inducing plasma expansion and the two target sides are both planar at the arrival of the main pulse. Therefore, we can suppose that protons are accelerated in both directions by a similar planar charge separation.

In Fig. 4(a), we see that the cut-off energy for the beam of ions increases linearly with laser pulse energy when using a constant ultra-short laser pulse of 30 fs. This linear trend, which is shown on Fig. 4(a) for front-side and rear side protons, is in good agreement with previous results obtained at other facilities in similar conditions. For example, in Zeil *et al.*,[37] the maximum proton energy obtained (17 MeV) is higher than what could be obtained here due to a higher encircled energy in their focal spot and a smaller focal spot diameter, leading to their higher on-target intensity (6×10^{20} W · cm^{-2}). Moreover, results obtained in our conditions and shown in Fig. 4(a) differ significantly from trends observed elsewhere, using longer-pulse duration, for which

the maximum proton energy is seen to vary as the square root of the laser energy (with fixed laser pulse duration).[4] This shows that proton acceleration is more dependent on the laser beam energy for short (<100 fs) laser pulses.

In the subsequent results, we take use of this observed linear dependence of maximum proton-energy on the laser energy to artificially correct for shot-to-shot fluctuations in laser pulse energy, which is of the order of 15%. In this, we recast our data to first order, from the systematic dependence of proton cut-off energy on laser-pulse energy: whenever a shot is higher or lower than 1.8 J, we correspondingly rescaled the measured proton cut-off energy-value down or up, respectively. This is internally consistent, and the resulting correction in the proton energy measured values is below 10%.

In Figure 4(b), the proton beam cut-off energy is plotted as a function of laser pulse duration, keeping the laser intensity constant and equal to $6.1 \times 10^{18}\,\mathrm{W \cdot cm^{-2}}$. We can observe that the proton beam cut-off energy increases with the laser pulse duration up to a few hundreds of fs, after which it becomes nearly constant. The obtained result is in agreement with Fuchs *et al.*,[22] and with models of expansion into vacuum of isothermal plasma driven by a hot electron component.[38] In these models, the maximum proton energy produced can be described as:

$$E_{max} = 2 \times T_{hot}[\ln(t_p + (t_p^2 + 1)^{1/2})]^2,$$

where $t_p = \frac{\omega_{pi} t_{acc}}{(2\exp 1)^{1/2}}$ is the normalized ion acceleration time, and T_{hot} is the hot electron temperature that drives the rear-surface plasma expansion. t_p is normalized using the ion plasma frequency $\omega_{pi} = \left[\frac{Z_i \times e^2 \times n_{e0}}{m_i \times \epsilon_0}\right]^{1/2}$, where Z_i and m_i are, respectively, the ion charge number and the mass, e is the electron charge, ϵ_0 is the electric permittivity in vacuum, and n_{e0} is the hot-electron density. The finite acceleration time t_{acc} is the time over which ion acceleration is considered to take place, after which electrons cool down and acceleration stops. One can approximate that the acceleration time is linked to the laser pulse duration by $t_{acc} \sim 1.3 \times \tau_{laser}$ when using a long laser pulse lasting a fraction of a picosecond ($\sim$0.3 ps).[22]

For shorter laser pulses duration, it is more appropriate to consider[39,40] that $t_{acc} \propto (\tau_{laser} + t_{min})$, where t_{min} is the energy exchange time between electrons and protons.[41] This exchange time depends on laser intensity and target thickness because it depends on the hot electron energy and the bounce frequency of the hot electrons between the target surfaces. This energy exchange time has been estimated to be at least 60 fs, and perhaps as large as 100 fs.[39,40] These estimations have been made using a 1D isothermal model for plasma expansion. Although a 1D isothermal model is a rather simple approximation to the actual 3D behaviour, which is at first isothermal and then later adiabatic,[19] it has been shown to be quite suitable to model experimental results of proton acceleration in the TNSA mechanism and for laser pulse-durations lasting 40 fs to 10 ps.[22,42]

Figure 5 shows the observed proton cut-off energy as a function of the target thickness, for the target front- and rear-side (Figs. 5(a) and 5(b), respectively). The proton cut-off energy is found for a laser pulse duration of 30 fs (full dots) and 100 fs (empty dots), while keeping E_{laser} fixed, and permitting I_{laser} to change. As shown in Fig. 5, as the target thickness is reduced, the maximum proton-energy increases for both proton directions (forward and backward), and this for two different laser pulse-durations. This shows that laser-accelerated hot electrons contribute more efficiently to proton acceleration when targets are thinner: since their longitudinal transit within the target is shorter, they lose less energy when recirculating within the target.[35,43] The electrons can bounce back and forth between the target front and rear sheaths for longer times in thinner targets, thereby increasing the effective sheath density that is setting up the electrostatic potential driving the acceleration mechanism. Moreover, when going to ultra thin targets, laser-plasma absorption is more efficient due to target decompression, which allows more efficient volume-heating of the electrons, and ultimately an improvement of the proton beam cut-off energy. It should be noted that our laser pulse contrast ratio in this experiment is high enough to permit the use of ultra thin targets as thin as 15 nm.

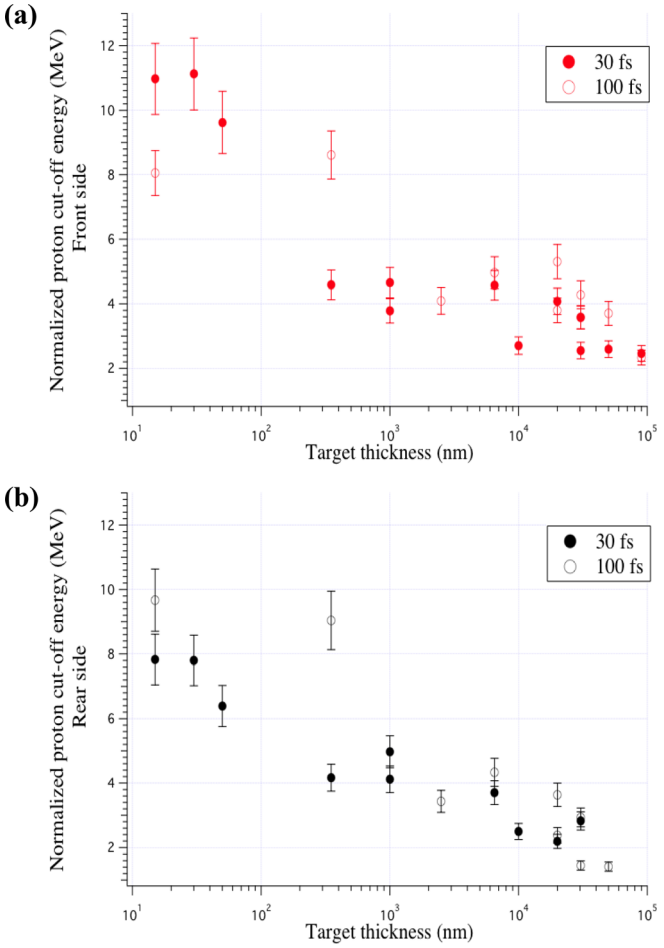

FIG. 5. Proton beam cut-off energy versus target thickness. The maximum energy is shown for two different pulse durations (30 fs and 100 fs). Plotted proton energies are rationalized to $E_{laser} = 1.8$ J, as described in the text.

Although there are shot-to-shot fluctuations of the proton cut-off energy, the trends observed in Fig. 5 for particles accelerated in the forward and backward directions do not

seem to differ significantly. However, one can observe that the proton maximum energy is generally higher for particles traveling in the backward direction (i.e., against the impinging laser beam). This result could be explained by ponderomotive pressure on the irradiated side, inhibiting the plasma expansion and keeping the sheath more confined than on its rear side, which may lead to greater proton acceleration.

Interestingly, Figure 5 does not exhibit any abrupt change in the maximum energy of protons accelerated from both sides of the target, when varying the target thickness, but instead rather a smooth drop-off with increasing target thickness. This suggests that we do not see a qualitative transition from TNSA, dominant for thick targets, to other potential mechanisms (RPA[44] or BOA[28–30]) that could dominate for ultra-thin targets. Notably, the similarities of plasma generation from front and rear sides, seen in shadowgraphy, are also preserved, going from thin to ultra-thin targets. It might be expected that RPA and BOA could lead to bulk movement of plasma forward, through the rear side and onward.

We still observe in Figure 5 that the maximum energy of protons accelerated from the target rear and front side is not significantly decreased when increasing the laser pulse-length, although fixing the laser pulse-energy at 1.8 J implies a reduction of the on-target laser intensity. Note that this case is different from the one shown in Fig. 4(b), where the laser pulse duration is varied while keeping the laser intensity constant (i.e., the laser pulse-energy is deliberately increased or decreased accordingly). From this, we can deduce that using the highest intensity level, i.e., the shortest pulse duration, does not necessarily yield the highest proton beam energy.

To study the impact of laser pulse duration in more detail than 30 fs versus 100 fs, we systematically varied the laser pulse duration (while holding the pulse energy constant, as in Fig. 5), using a single target-thickness of 120 nm. The results are given in Figure 6 for the target front-side and the target rear-side (Figs. 6(a) and 6(b), respectively). In Fig. 6(a), we observe a smooth maximum for the proton cut-off energy versus laser pulse duration. This trend appears for electrons accelerated in the backward direction, when using a pulse duration of 100 ± 50 fs. This behaviour is not observed in the forward direction (Fig. 6(b)), and in this case, the proton energy is not significantly higher for the shortest laser pulse duration. Similar results, albeit at lower laser intensity, are detailed in Flacco *et al.*,[45] and suggest an optimal laser pulse duration and target thickness for these laser conditions. In previous works, this optimum is a compromise between supplying the highest possible laser intensity and the efficiency with which that intense light can be coupled into the laser-produced plasma.[45,46] Indeed, on one hand, when there is a large plasma gradient on the target front-side (as characteristic of long-pulse laser irradiation), typical mechanisms of absorption include inverse Bremsstrahlung, and parametric processes that deposit energy into relatively few electrons at low density and at greater distance from the solid foil, and bulk of electrons. Brunel absorption is not an important mechanism. On the other hand, for the shortest pulses and with ultra-high laser contrast, the plasma has little time to expand at all. Brunel absorption is again

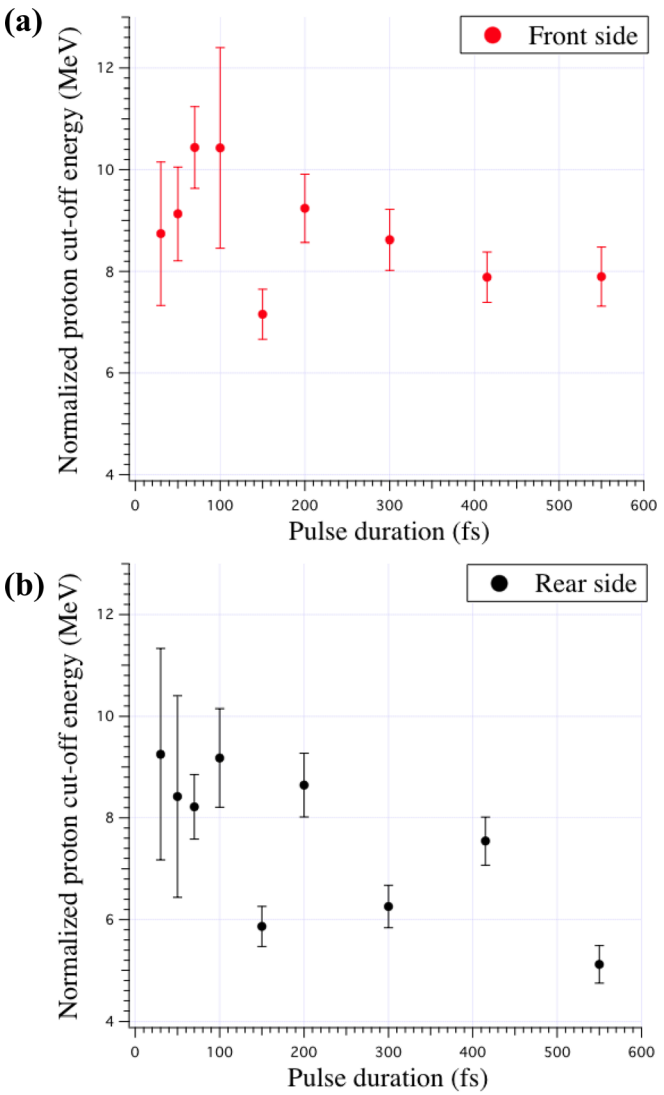

FIG. 6. Proton beam cut-off energy as a function of the laser pulse duration. The targets thickness is 110 nm. The reported proton cut-off energy is normalized to $E_{laser} = 1.8$ J.

minimized, and Fresnel reflection at the abrupt discontinuity is increased. Again, little energy is coupled into the electrons needed to populate the sheath needed for TNSA. A description of absorption processes at high intensity, and with different scale-lengths can be found in Geindre *et al.*[47,48]

The plasma gradient that exists on the target surface is not only of importance for laser-plasma coupling and laser absorption. It is in itself a crucial parameter in the proton acceleration TNSA mechanism.[19] Indeed, the charge separation, which drives the proton acceleration, is proportional to $(n_{hot} \times T_{hot})^{1/2}$ when the plasma scale length l_g is below the hot electron Debye length λ_d.[38] However, it is reduced to $\frac{T_{hot}}{l_g}$ when $l_g > \lambda_d$.[19,49] This is the case for long laser pulse durations, which induce longer gradient plasmas. Another effect associated with long laser pulse durations is that later in the laser pulse, the cold electrons generated by the laser reduce the effect of hot electrons establishing the ambipolar potential. In this sense, long laser pulses, which inject in the plasma a proportion of electrons late in time, will be less efficient for proton acceleration.

For very thin targets, it is important to notice that the issues related to plasma gradients become less of a concern since the effective electron sheath density is higher than for a thick target, due to refluxing. This high electron density, produced by the fast longitudinal electron recirculation, decreases the Debye length on the target surfaces. Hence, relative to such short Debye length, high plasma gradient lengths cannot be tolerated without being detrimental to proton acceleration.

IV. CONCLUSION

We report the investigation of laser-driven proton acceleration, for a range of experimental parameters available from a single ultrafast Ti:sapphire laser system. When using ultra-short laser pulses, the optimum proton acceleration that can be produced by TNSA will result from a compromise between laser absorption, laser intensity and target surfaces expansion. This compromise is related to the electron temperature and the laser absorption, i.e., laser-plasma coupling and plasma expansion in the acceleration sheath. We show that using such laser system, optimization is achieved using a target thickness close to 30 nm, and 100 fs laser pulse duration combined with the maximum available laser energy.

ACKNOWLEDGMENTS

The authors would like to thanks the ALLS technical team for their support: M. O. Bussière, J. Maltais, C. Morissette, L. Pelletier, F. Poitras, P. L. Renault, and C. Sirois. The ALLS facility has been funded by the Canadian Foundation for Innovation (CFI). This work was funded by NSERC and the Canada Research Chair program.

[1]A. Rousse, C. Rischel, S. Fourmaux, I. Uschmann, S. Sebban, G. Grillon, Ph. Balcou, E. Forster, J. P. Geindre, P. Audebert, J. C. Gauthier, and D. Hulin, "Non-thermal melting in semiconductors measured at femtosecond resolution," Nature **410**(6824), 65–68 (2001).

[2]S. Fourmaux, S. Corde, K. Ta Phuoc, P. Lassonde, G. Lebrun, S. Payeur, F. Martin, S. Sebban, V. Malka, A. Rousse, and J. C. Kieffer, "Single shot phase contrast imaging using laser-produced Betatron x-ray beams," Opt. Lett. **36**(13), 2426–2428 (2011).

[3]C. Rechatin, J. Faure, A. Ben-Ismail, J. Lim, R. Fitour, A. Specka, H. Videau, A. Tafzi, F. Burgy, and V. Malka, "Controlling the phase-space volume of injected electrons in a laser-plasma accelerator," Phys. Rev. Lett. **102**(16), 1–4 (2009).

[4]M. Borghesi, J. Fuchs, S. V. Bulanov, A. J. Mackinnon, P. K. Patel, and M. Roth, "Fast ion generation by high-intensity laser irradiation of solid targets and applications," Fusion Sci. Technol. **49**(3), 412–439 (2006).

[5]R. Fedosejevs, I. V. Tomov, N. H. Burnett, G. D. Enright, and M. C. Richardson, "Self-steepening of the density profile of a co_2-laser-produced plasma," Phys. Rev. Lett. **39**, 932–935 (1977).

[6]N. A. Ebrahim, C. Joshi, D. M. Villeneuve, N. H. Burnett, and M. C. Richardson, "Anomalous energy transport to rear surface of microdisks at high laser irradiances," Phys. Rev. Lett. **43**, 1995–1998 (1979).

[7]R. S. Marjoribanks, M. D. J. Burgess, G. D. Enright, and M. C. Richardson, "Propagation of the superthermal corona from co_2-laser-irradiated microtargets," Phys. Rev. Lett. **45**, 1798–1801 (1980).

[8]R. A. Snavely, M. H. Key, S. P. Hatchett, T. E. Cowan, M. Roth, T. W. Phillips, M. A. Stoyer, E. A. Henry, T. C. Sangster, M. S. Singh, S. C. Wilks, A. MacKinnon, A. Offenberger, D. M. Pennington, K. Yasuike, A. B. Langdon, B. F. Lasinski, J. Johnson, M. D. Perry, and E. M. Campbell, "Intense high-energy proton beams from Petawatt-laser irradiation of solids," Phys. Rev. Lett. **85**(14), 2945–2948 (2000).

[9]S. P. Hatchett, C. G. Brown, T. E. Cowan, E. A. Henry, J. S. Johnson, M. H. Key, J. A. Koch, A. B. Langdon, B. F. Lasinski, R. W. Lee, A. J. Mackinnon, D. M. Pennington, M. D. Perry, T. W. Phillips, M. Roth, T. C. Sangster, M. S. Singh, R. A. Snavely, M. A. Stoyer, S. C. Wilks, and K. Yasuike, "Electron, photon, and ion beams from the relativistic interaction of Petawatt laser pulses with solid targets," Phys. Plasmas **7**(5), 2076–2082 (2000).

[10]M. Hegelich, S. Karsch, G. Pretzler, D. Habs, K. Witte, W. Guenther, M. Allen, A. Blazevic, J. Fuchs, J. Gauthier, M. Geissel, P. Audebert, T. Cowan, and M. Roth, "MeV ion jets from short-pulse-laser interaction with thin foils," Phys. Rev. Lett. **89**(8), 19–22 (2002).

[11]T. Cowan, J. Fuchs, H. Ruhl, A. Kemp, P. Audebert, M. Roth, R. Stephens, I. Barton, A. Blazevic, E. Brambrink, J. Cobble, J. Fernández, J.-C. Gauthier, M. Geissel, M. Hegelich, J. Kaae, S. Karsch, G. Le Sage, S. Letzring, M. Manclossi, S. Meyroneinc, A. Newkirk, H. Pépin, and N. Renard-LeGalloudec, "Ultralow emittance, multi-MeV proton beams from a laser virtual-cathode plasma accelerator," Phys. Rev. Lett. **92**(20), 1–4 (2004).

[12]J. Fuchs, T. Cowan, P. Audebert, H. Ruhl, L. Gremillet, A. Kemp, M. Allen, A. Blazevic, J.-C. Gauthier, M. Geissel, M. Hegelich, S. Karsch, P. Parks, M. Roth, Y. Sentoku, R. Stephens, and E. Campbell, "Spatial uniformity of laser-accelerated ultrahigh-current MeV electron propagation in metals and insulators," Phys. Rev. Lett. **91**(25), 2–5 (2003).

[13]M. Borghesi, D. H. Campbell, A. Schiavi, M. G. Haines, O. Willi, A. J. MacKinnon, P. Patel, L. A. Gizzi, M. Galimberti, R. J. Clarke, F. Pegoraro, H. Ruhl, and S. Bulanov, "Electric field detection in laser-plasma interaction experiments via the proton imaging technique," Phys. Plasmas **9**(5), 2214 (2002).

[14]P. K. Patel, A. Mackinnon, M. H. Key, T. E. Cowan, M. E. Foord, M. Allen, D. F. Price, H. Ruhl, P. T. Springer, and R. Stephens, "Isochoric heating of solid-density matter with an ultrafast proton beam," Phys. Rev. Lett. **91**(12), 10–13 (2003).

[15]J. J. Honrubia, J. C. Fernández, M. Temporal, B. M. Hegelich, and J. Meyer-ter Vehn, "Fast ignition by laser-driven carbon beams," J. Phys.: Conf. Ser. **244**(2), 022038 (2010).

[16]I. Spencer, K. W. D. Ledingham, R. P. Singhal, T. McCanny, P. McKenna, E. L. Clark, K. Krushelnick, M. Zepf, F. N. Beg, M. Tatarakis, A. E. Dangor, P. A. Norreys, R. J. Clarke, R. M. Allott, and I. N. Ross, "Laser generation of proton beams for the production of short-lived positron emitting radioisotopes," Nucl. Instrum. Meth. Phys. Res. B **183**(3–4), 449–458 (2001).

[17]F. Pegoraro, S. Atzeni, M. Borghesi, S. Bulanov, T. Esirkepov, J. Honrubia, Y. Kato, V. Khoroshkov, K. Nishihara, T. Tajima, M. Temporal, and O. Willi, "Production of ion beams in high-power laser-plasma interactions and their applications," Laser Part. Beams **3**(1), 19–24 (2004).

[18]S. C. Wilks, A. B. Langdon, T. E. Cowan, M. Roth, M. Singh, S. Hatchett, M. H. Key, D. Pennington, A. MacKinnon, and R. A. Snavely, "Energetic proton generation in ultra-intense laser-solid interactions," Phys. Plasmas **8**(2), 542 (2001).

[19]T. Grismayer and P. Mora, "Influence of a finite initial ion density gradient on plasma expansion into a vacuum," Phys. Plasmas **13**(3), 032103 (2006).

[20]S. J. Gitomer, R. D. Jones, F. Begay, A. W. Ehler, J. F. Kephart, and R. Kristal, "Fast ions and hot electrons in the laser-plasma interaction," Phys. Fluids **29**(8), 2679–2688 (1986).

[21]S. A. Gaillard, T. Kluge, K. A. Flippo, M. Bussmann, B. Gall, T. Lockard, M. Geissel, D. T. Offermann, M. Schollmeier, Y. Sentoku, and T. E. Cowan, "Increased laser-accelerated proton energies via direct laser-light-pressure acceleration of electrons in microcone targets," Phys. Plasmas **18**(5), 056710 (2011).

[22]J. Fuchs, P. Antici, E. d'Humières, E. Lefebvre, M. Borghesi, E. Brambrink, C. A. Cecchetti, M. Kaluza, V. Malka, M. Manclossi, S. Meyroneinc, P. Mora, J. Schreiber, T. Toncian, H. Pépin, and P. Audebert, "Laser-driven proton scaling laws and new paths towards energy increase," Nature Phys. **2**(1), 48–54 (2005).

[23]T. Esirkepov, M. Borghesi, S. Bulanov, G. Mourou, and T. Tajima, "Highly efficient relativistic-ion generation in the laser-piston regime," Phys. Rev. Lett. **92**(17), 2–5 (2004).

[24]O. Klimo, J. Psikal, J. Limpouch, and V. Tikhonchuk, "Monoenergetic ion beams from ultrathin foils irradiated by ultrahigh-contrast circularly polarized laser pulses," Phys. Rev. ST Accel. Beams **11**(3), 1–14 (2008).

[25]A. Henig, S. Steinke, M. Schnürer, T. Sokollik, R. Hörlein, D. Kiefer, D. Jung, J. Schreiber, B. M. Hegelich, X. Q. Yan, J. Meyer-ter Vehn, T. Tajima, P. V. Nickles, W. Sandner, and D. Habs, "Radiation-pressure acceleration of ion beams driven by circularly polarized laser pulses," Phys. Rev. Lett. **103**(24), 3–6 (2009).

[26]A. Macchi, S. Veghini, and F. Pegoraro, "'Light Sail' acceleration reexamined," Phys. Rev. Lett. **103**(8), 1–4 (2009).
[27]F. Dollar, C. Zulick, A. G. R. Thomas, V. Chvykov, J. Davis, G. Kalinchenko, T. Matsuoka, C. McGuffey, G. M. Petrov, L. Willingale, V. Yanovsky, A. Maksimchuk, and K. Krushelnick, "Finite spot effects on radiation pressure acceleration from intense high-contrast laser interactions with thin targets," Phys. Rev. Lett. **108**(17), 1–5 (2012).
[28]L. Yin, B. J. Albright, B. M. Hegelich, and J. C. Fernández, "GeV laser ion acceleration from ultrathin targets: The laser break-out afterburner," Laser Part. Beams **24**(2), 291–298 (2006).
[29]L. Yin, B. J. Albright, B. M. Hegelich, K. J. Bowers, K. A. Flippo, T. J. T. Kwan, and J. C. Fernández, "Monoenergetic and GeV ion acceleration from the laser breakout afterburner using ultrathin targets," Phys. Plasmas **14**(5), 056706 (2007).
[30]B. J. Albright, L. Yin, Kevin J. Bowers, B. M. Hegelich, K. A. Flippo, T. J. T. Kwan, and J. C. Fernández, "Relativistic Buneman instability in the laser breakout afterburner," Phys. Plasmas **14**(9), 094502 (2007).
[31]S. Fourmaux, S. Payeur, A. Alexandrov, C. Serbanescu, F. Martin, T. Ozaki, A. Kudryashov, and J.-C. Kieffer, "Laser beam wavefront correction for ultra high intensities with the 200 TW laser system at the advanced laser light source," Opt. Express **16**(16), 11987–11994 (2008).
[32]S. Fourmaux, S. Payeur, S. Buffechoux, P. Lassonde, C. St-Pierre, F. Martin, and J.-C. Kieffer, "Pedestal cleaning for high laser pulse contrast ratio with a 100 TW class laser system," Opt. Express **19**(9), 8486–8497 (2011).
[33]J. M. Mikhailova, A. Buck, A. Borot, K. Schmid, C. Sears, G. D. Tsakiris, F. Krausz, and L. Veisz, "Ultra-high-contrast few-cycle pulses for multipetawatt-class laser technology," Opt. Lett. **36**(16), 3145–3147 (2011).
[34]S. Nakamura, Y. Iwashita, A. Noda, T. Shirai, H. Tongu, A. Fukumi, M. Kado, A. Yogo, M. Mori, S. Orimo, K. Ogura, A. Sagiska, M. Nishiuchi, Y. Hayashi, Z. Li, H. Daido, and Y. Wada, "Real-time optimization of proton production by intense short-pulse laser with time-of-flight measurement," Jpn. J. Appl. Phys. **45**(34), L913–L916 (2006).
[35]E. Brambrink and M. Roth, "Modeling of the electrostatic sheath shape on the rear target surface in short-pulse laser-driven proton acceleration," Laser Part. Beams **24**(1), 163–168 (2006).
[36]T. Ceccotti, A. Lévy, H. Popescu, F. Réau, P. d'Oliveira, P. Monot, J. P. Geindre, E. Lefebvre, and Ph. Martin, "Proton acceleration with high-intensity ultrahigh-contrast laser pulses," Phys. Rev. Lett. **99**(18), 1–4 (2007).
[37]K. Zeil, S. D. Kraft, S. Bock, M. Bussmann, T. E. Cowan, T. Kluge, J. Metzkes, T. Richter, R. Sauerbrey, and U. Schramm, "The scaling of proton energies in ultrashort pulse laser plasma acceleration," New J. Phys. **12**(4), 045015 (2010).
[38]P. Mora, "Plasma expansion into a vacuum," Phys. Rev. Lett. **90**(18), 16–19 (2003).
[39]M. Carrié, E. Lefebvre, A. Flacco, and V. Malka, "Influence of subpicosecond laser pulse duration on proton acceleration," Phys. Plasmas **16**(5), 053105 (2009).
[40]J. Fuchs, Y. Sentoku, E. d'Humières, T. E. Cowan, J. Cobble, P. Audebert, A. Kemp, A. Nikroo, P. Antici, E. Brambrink, A. Blazevic, E. M. Campbell, J. C. Fernández, J.-C. Gauthier, M. Geissel, M. Hegelich, S. Karsch, H. Popescu, N. Renard-LeGalloudec, M. Roth, J. Schreiber, R. Stephens, and H. Pépin, "Comparative spectra and efficiencies of ions laser-accelerated forward from the front and rear surfaces of thin solid foils," Phys. Plasmas **14**(5), 053105 (2007).
[41]A. A. Andreev, R. Sonobe, S. Kawata, S. Miyazaki, K. Sakai, K. Miyauchi, T. Kikuchi, K. Platonov, and K. Nemoto, "Effect of a laser prepulse on fast ion generation in the interaction of ultra-short intense laser pulses with a limited-mass foil target," Plasma Phys. Controlled Fusion **48**(11), 1605–1619 (2006).
[42]L. Robson, P. T. Simpson, R. J. Clarke, K. W. D. Ledingham, F. Lindau, O. Lundh, T. McCanny, P. Mora, D. Neely, C.-G. Wahlström, M. Zepf, and P. McKenna, "Scaling of proton acceleration driven by petawatt-laser-plasma interactions," Nature Phys. **3**(1), 58–62 (2006).
[43]A. Mackinnon, Y. Sentoku, P. K. Patel, D. W. Price, S. Hatchett, M. Key, C. Andersen, R. Snavely, and R. R. Freeman, "Enhancement of proton acceleration by hot-electron recirculation in thin foils irradiated by ultraintense laser pulses," Phys. Rev. Lett. **88**(21), 1–4 (2002).
[44]A. Macchi, F. Cattani, T. Liseykina, and F. Cornolti, "Laser acceleration of ion bunches at the front surface of overdense plasmas," Phys. Rev. Lett. **94**(16), 2–5 (2005).
[45]A. Flacco, F. Sylla, M. Veltcheva, M. Carrié, R. Nuter, E. Lefebvre, D. Batani, and V. Malka, "Dependence on pulse duration and foil thickness in high-contrast-laser proton acceleration," Phys. Rev. E **81**(3), 036405 (2010).
[46]P. Antici, J. Fuchs, E. d'Humières, J. Robiche, E. Brambrink, S. Atzeni, A. Schiavi, Y. Sentoku, P. Audebert, and H. Pépin, "Laser acceleration of high-energy protons in variable density plasmas," New J. Phys. **11**(2), 023038 (2009).
[47]J. P. Geindre, P. Audebert, and R. S. Marjoribanks, "Relativistic *ac* gyromagnetic effects in ultraintense laser-matter interaction," Phys. Rev. Lett. **97**, 085001 (2006).
[48]J. P. Geindre, R. S. Marjoribanks, and P. Audebert, "Electron vacuum acceleration in a regime beyond Brunel absorption," Phys. Rev. Lett. **104**, 135001 (2010).
[49]J. Fuchs, C. A. Cecchetti, M. Borghesi, T. Grismayer, E. d'Humières, P. Antici, S. Atzeni, P. Mora, A. Pipahl, L. Romagnani, A. Schiavi, Y. Sentoku, T. Toncian, P. Audebert, and O. Willi, "Laser-foil acceleration of high-energy protons in small-scale plasma gradients," Phys. Rev. Lett. **99**, 015002 (2007).